LETTER TO THE EDITOR

Probing buried interfaces with soft x-ray standing wave spectroscopy: application to the Fe/Cr interface

See-Hun Yang[1]**, Bongjin S Mun**[1,2]**, Norman Mannella**[1,2]**,
Sang-Koog Kim**[3]**, Jeffrey B Kortright**[1]**, James Underwood**[1]**,
Farhad Salmassi**[1]**, Elke Arenholz**[4]**, Anthony Young**[4]**, Zahid Hussain**[4]**,
Michel A Van Hove**[1,2] **and Charles S Fadley**[1,2,5]

[1] Materials Sciences Division, Lawrence Berkeley Laboratory, Berkeley, CA 94720, USA
[2] Department of Physics, University of California at Davis, Davis, CA 95016, USA
[3] School of Materials Science and Engineering, College of Engineering Seoul National
University, Seoul 151-744, Korea
[4] Advanced Light Source, Lawrence Berkeley Laboratory, Berkeley, CA 94720, USA
[5] Department of Physics, University of Hawaii, Honolulu, HI 96822, USA

Abstract
The nanometre-scale materials and devices that are under ever more intense
study at present often depend for their unique properties on buried interfaces
between two phases. Yet the number of experimental techniques that can
specifically probe such interfaces, particularly with magnetic sensitivity,
is limited. We here report a novel type of non-destructive method for
spectroscopically studying buried nanometre-scale interfaces and other
nanostructures with soft x-ray standing waves. Strong standing waves with
a period of 4.0 nm and approximately 3:1 contrast ratios are created via Bragg
reflection from a synthetic multilayer of form $[B_4C/W]_{40}$. By growing a wedge-
shaped Fe/Cr bilayer on top of this multilayer, the mechanical translation of
the bilayer exposed to a fixed and finely focused synchrotron radiation beam
is converted into a translation of the standing wave through the interface.
Analysing various core photoelectron intensities as a function of angle and beam
position permits derivation of layer thicknesses and interface mixing/roughness
scales. Magnetic circular dichroism in photoemission from the 2p and 3p levels
of Fe and Cr further permits derivation of the positions and widths of regions
with decreased (increased) ferromagnetic alignment for Fe (Cr), showing that
normally antiferromagnetic Cr becomes ferromagnetic just below the centre
of the interface but with antiparallel alignment with respect to Fe, and that
the equal-concentration region in the centre of the interface strongly inhibits
magnetic alignment for both species along the direction of net magnetizations
that is probed. The magnetically altered regions in both metals are only 1–2
atomic layers in thickness. 3s spectra from Fe and Cr further indicate that the
local spin moments on both atoms do not change on crossing the interface. This
standing-wave-plus-wedge method should have a range of applications for the
characterization of nanostructures and their interfaces.

(Some figures in this article are in colour only in the electronic version)

Many current technological devices consist of layered or sandwich structures, the thickness of whose composite layers is either already in the nanometre (10 Å) range or in the process of shrinking into the nanometre range. These devices include transistors in integrated circuits, solid-state lasers and magnetic elements for storing information and for reading it out. Such interfaces may exhibit intermixing of the components on either side and/or roughness, as well as altered chemical states or states of magnetic order, and their exact nature can affect ultimate properties such as electrical conductivity or magnetic stability in a profound way. As one example of such nanostructures in magnetism, the phenomenon of giant magnetoresistance (GMR) is based on the change in resistance in a sandwich structure consisting of alternating non-magnetic and magnetic layers upon being exposed to an external magnetic field [1, 2]. GMR is today used routinely in the read heads for highest-density information storage, where it is usually combined with another interface-driven effect, exchange biasing [3]. Magnetic tunnel junctions have similar properties and are promising for magnetic random access memory and terabyte-scale hard disk storage device applications [4]. Since interfaces are believed to play a pivotal role in the behaviour of all of these effects, extensive theoretical and experimental work has been carried out in order to unveil the physical and chemical nature of them [1–4]; nonetheless, many fundamental questions remain. Numerous other examples of important interfaces are found, for example in semiconductor science and technology. Beyond this are also various nanometre-scale tubes, wires and clusters which can have buried or hidden interfaces where they make contact with some kind of supporting substrate or with themselves.

It is thus of interest to develop new, non-destructive, element-specific, spectroscopic tools for studying the buried interfaces in such nanostructures. Some of the questions to answer with such a probe are: What are the positions and thicknesses of the compositional intermixing or magnetic transition layers across the interface? What is the roughness of the interface, both chemical and magnetic? What are the chemical and magnetic states of the various atoms involved as a function of position perpendicular to the interface? How does the valence electronic structure and density of electronic states vary across the interface? How does both the short-range and long-range magnetic order depend on position relative to the interface?

Some of these questions can be answered at least partially using currently available methods, and we briefly mention a few of these. One powerful method is scanning transmission electron microscopy (STEM) with electron energy loss spectroscopy (EELS) [5], but this technique requires specialized sample slicing and thinning and thus cannot be considered non-destructive, and in its most sophisticated element-specific form with EELS still cannot provide both element specificity and magnetic sensitivity at the sub-nanometre scale. Hard x-rays in the 5–10 keV range can be reflected from buried interfaces and planar multilayer nanostructures so as to set up standing waves that may permit depth-dependent composition, structure and, via variable light polarization or magnetization direction, also magnetism near buried interfaces to be derived [6,7]. But these hard x-ray measurements are limited as to both energy resolution and spectroscopic characterization, and also may due to their shorter wavelengths (∼1–2 Å) exhibit interference structures from atomic lattice planes that can be much smaller than the nanometre scale it is desired to probe. Another method uses total reflection of soft x-rays in the 0.5–1.5 keV range from a buried interface by tuning the photon energy to a core-level absorption edge [8], and this can determine both chemical and magnetic roughness by working with both right and left circularly polarized radiation (RCP and LCP, respectively) and/or flipping the sample magnetization $\vec{M}$ between two orientations 1 and 2 and measuring a magnetic asymmetry in diffuse reflectivity as $\Delta R_{MCD} \propto R_{RCP} - R_{LCP}$ or $\propto R_{M1} - R_{M2}$. However, this method does not permit detailed spectroscopic studies (e.g. via photoelectron emission) of the buried interface. Finally, soft x-ray spectromicroscopy using secondary electrons as the detecting

medium can achieve some sensitivity to buried interfaces, provided that there are sufficient chemical fingerprints in the x-ray absorption signal to deconvolve the interface contributions to images [9]. However, any method using lower-energy electrons to study buried interfaces is inherently limited by the short inelastic attenuation lengths in the 1–5 nm range, which strongly attenuate the signals.

We here focus on a novel approach making use of photoelectrons (or in future applications also fluorescent soft x-rays) excited by strong *soft x-ray* standing waves that are set up in Bragg reflection from a synthetic multilayer structure of a few nanometres in periodicity. This multilayer is in turn used as the substrate and sample preparation surface in the experiment. Soft x-rays in the 0.5–1.5 keV range have much higher cross sections for exciting outer-shell photoelectrons or fluorescent x-rays than harder x-rays, and these can in turn be analysed with resolutions in the $1:10^3$ or $1:10^4$ range via suitable spectrometers. By either varying the angle of incidence around the Bragg angle or varying the thickness of the sample on top of the multilayer, the standing wave and the spectroscopy which it excites can effectively be scanned through the interface, thus providing additional depth sensitivity and a method for non-destructively probing chemical composition, chemical state, structure and magnetism through a given interface. Some preliminary aspects of this soft x-ray standing wave approach involving both photoelectron emission [10] and x-ray absorption [11] have been discussed recently. In the present work, we add two key elements: a wedge-shaped (tapered) sample to provide the most unambiguous method of probing the interface, and measurements including magnetic circular dichroism (MCD) and spin-sensitive core-level spectroscopy.

Our basic approach is illustrated in figure 1(a) for the specific example of an Fe/Cr bilayer grown on a B_4C/W multilayer structure consisting of 40 bilayers of period $d = 40.5$ Å. A beam of monochromatized soft x-ray synchrotron radiation at 825.0 eV (wavelength $\lambda_x = 15.0$ Å) emitted from a high-brightness elliptically polarized undulator at the Advanced Light Source in Berkeley is focused down to a spot of about 0.2 mm in diameter, and is incident on the surface of an Fe/Cr bilayer consisting of a wedge-shaped Cr underlayer with thickness varying from 118 Å at one end to 36 Å at the other end and an Fe overlayer with a constant thickness of 16.0 Å. Strong Bragg reflection from the planes in the multilayer will occur when the x-ray incidence angle $\theta_{h\nu}$ satisfies $n\lambda_x \approx 2d \sin \theta_{h\nu}$, with $n = 1, 2, 3, \ldots$ the order of the reflection. For the strongest reflection at $n = 1$, the resulting standing wave has a period equal to d (in our case thus 40.5 Å = 4 nm) and it will extend many nanometres above the surface of the multilayer.

We have chosen to study the Fe/Cr interface as a first demonstration case because of its importance in GMR, since multilayers of these two materials exhibit one of the highest values for magnetoresistance [1]. It is thus a prototype system for this effect, even though it is not used in actual commercial devices, and its properties have been extensively studied [12–19]. The Fe/Cr interface also is known from prior spectroscopy [12, 13], scanning tunnelling microscopy (STM) [14, 15], x-ray diffraction [15] and theoretical modelling [16–18] studies to involve a variable degree of intermixing, depending on exactly how it is grown. It has also been shown from MCD studies in x-ray absorption and photoelectron emission that Cr, which is normally antiferromagnetic, becomes ferromagnetically ordered to some degree near the interface, but anti-parallel to the Fe magnetization, and from this and other work that the Cr magnetic moment may be significantly increased, at least near free surfaces as an overlayer [12, 13, 19]. Also, the degree of ferromagnetic order of Fe, or perhaps its local atomic magnetic moment, is thought to be reduced near the interface [19]. However, much prior work has involved very thin films [12, 13, 17, 19], starting with a single or partial monolayer of Cr and growing upward from there; thus, it is still not clear as to what occurs at a truly buried interface. Our goal here is to directly probe this interface with core-level photoelectron spectroscopy
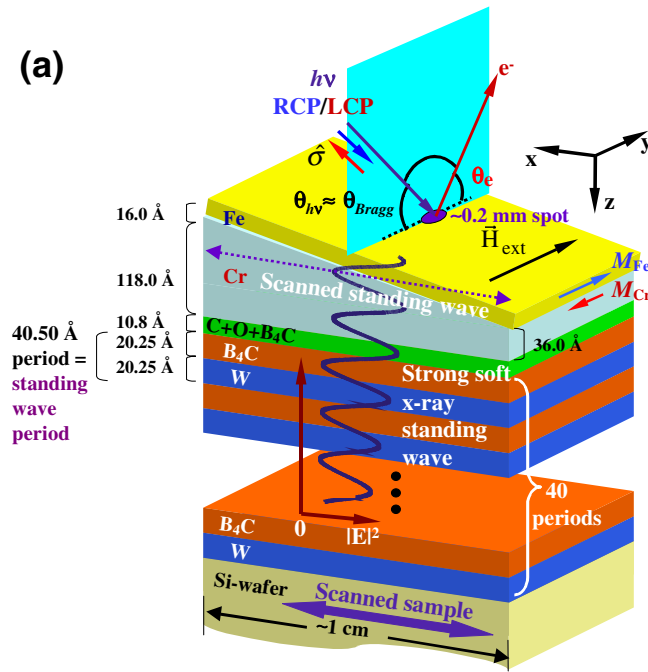
Figure 1. (a) Schematic diagram of our experimental geometry, including a wedge-shaped Fe/Cr bilayer on top of a synthetic multilayer standing wave generator. Note the Cartesian axes, with magnetization along y and the sample scanned along x. (b) Core-level photoemission intensity ratios $I(Cr\ 3p)/I(Fe\ 3p)$ as a function of x-ray incidence angle θ_{hv} and Cr wedge thickness d_{Cr} (lines and symbols), together with best-fit calculations (solid curves). (c) The calculated depth-dependent electric field strength $|E|^2$ as a function of d_{Cr}, together with interdiffusion widths at various interfaces (2σ) as derived in this study. The σ for the interface between B_4C and W was determined from hard x-ray reflectometry, while the others were obtained from our analysis of soft x-ray standing-wave photoemission data (see text). Positions B and C are special in that the crest (B) and trough (C) of the standing wave are situated on the Fe–Cr interface, respectively.

as excited by a standing wave, and to make use of both Fe and Cr core spectra, as well as MCD in them, to more quantitatively study the interface compositional mixing/roughness, the individual magnetic moments on both Fe and Cr through the interface and the type and spatial distribution of magnetic order in both constituents through the interface.

Prior to evaporation of Cr and Fe, the structural parameters and reflectivities of the $[B_4C/W]_{40}$ standing-wave generator (SWG) have been measured via standard hard x-ray reflectometry at 8.05 keV, with a theoretical analysis of these data yielding the period d of 40.5 Å and a Gaussian interface interdiffusion length between the two components of $\sigma^{B4C/W} = 4.1$ Å. The top surface of the multilayer (which was air exposed before being inserted into ultrahigh vacuum for Cr and Fe deposition) was also characterized by both STM and atomic force microscopy (AFM), and found to be very smooth, with an average roughness of about 3.0 Å and a root-mean-square (RMS) roughness of about 5 Å.

Cr and Fe layers were then deposited on this top surface from Knudsen-type evaporation cells, at ambient pressures of $1-2 \times 10^{-10}$ Torr; scanning the sample in the x-direction during growth produced the desired Cr wedge. All bilayer preparation and measurement was done in the advanced photoelectron spectrometer/diffractomer [20] situated on undulator beamline 4.0.2 at the Berkeley Advanced Light Source [21], with the beamline providing
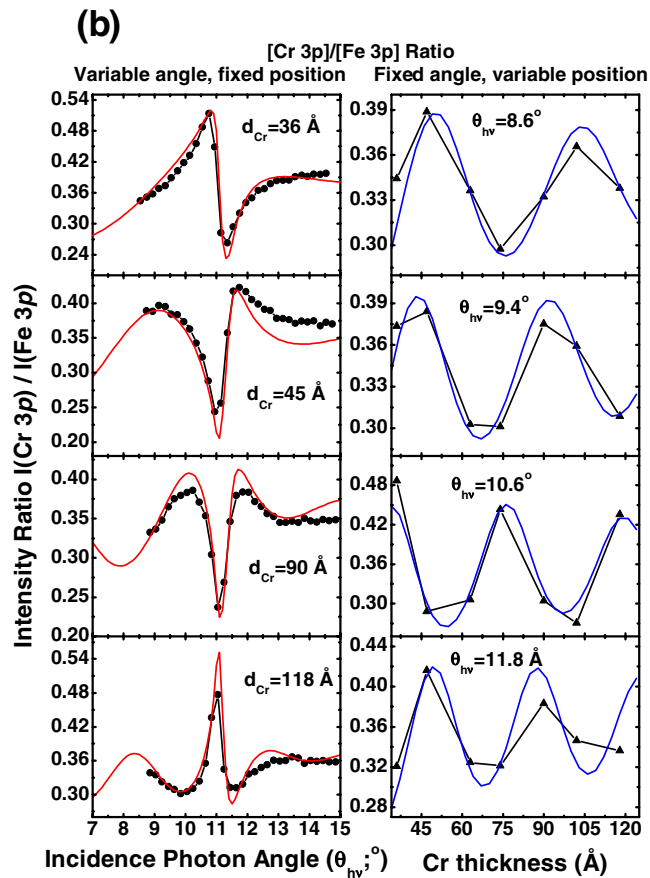
(b)

Figure 1. (Continued.)

high-brightness variable-polarization radiation in the soft x-ray range. The Cr/Fe overlayers were polycrystalline or amorphous, as verified by the lack of structure in core photoelectron diffraction patterns. The pressures during subsequent spectroscopic measurements were in the 1×10^{-10} range, with little contamination buildup on the top surface as judged by C 1s and O 1s photoelectron spectra (<2 atomic layers in 24 h). The Fe layer was initially magnetized in plane along the y direction (cf figure 1(a)) by subjecting it to an external field of about 500 Oe. The radiation polarization could be varied from linear polarized (LP) to right circular polarized (RCP) or left circular polarized (LCP) via the undulator involved [21].

As a first measurement procedure, scanning the x-ray incidence angle around the expected first-order Bragg angle for the bare multilayer or multilayer + wedge, thus tracing out its 'rocking curve', and comparing the resulting angular-dependent core-level photoelectron intensities from each constituent (Fe 2p and 3p, Cr 2p and 3p, B 1s, C 1s and W 4f) with theoretical calculations based on classical x-ray optics [10] permits determination of the Bragg angle with high accuracy. For the particular sample studied here, it is $11.05° \pm 0.10°$, in excellent agreement with theoretical calculations, and very close to the $10.70°$ calculated from the simple formula above. The discrepancy of $0.35°$ is due to refraction and phase shifts in the waves reflected and refracted at each of the interfaces involved, as a result of the small deviations from unity of the complex optical constants (n_i) in each layer [22]. For the
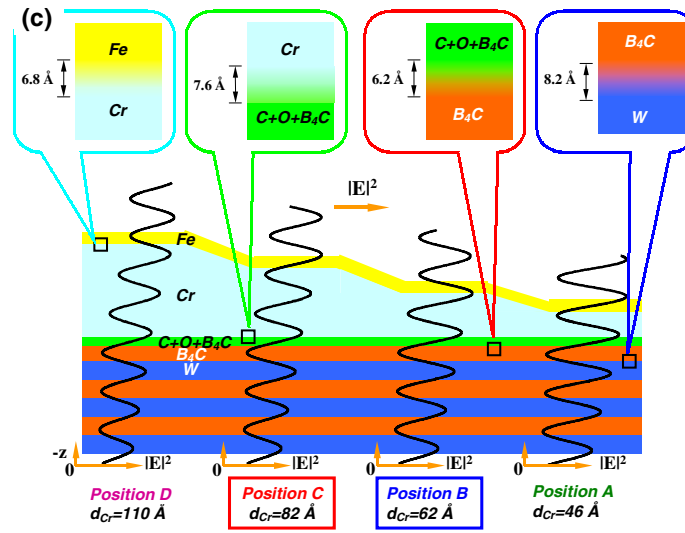
Figure 1. (Continued.)

measurements discussed here, the photon incidence angle and energy were fixed at 11.05°
and 825 eV, respectively, with this energy also being far away from any Fe, Cr, B, C, W or O
absorption edges.

For these conditions, we have also verified via measurements and theoretical simulations
not shown here that the Bragg angle and the phase of the standing wave with respect to the
top surface of the multilayer are negligibly altered by the presence of the Fe/Cr bilayer, as
judged relative to a native multilayer with no overlayer on top of it [23]. Thus, as our primary
measurement procedure, simply moving the sample back and forth along the axis of the slope
of the wedge (the x axis in figure 1(a)) will scan the focused x-ray beam along the wedge, but
with the net effect also of scanning the fixed-phase standing wave through the buried Fe/Cr
interface. In this mode, the number of unknown parameters in the analysis of the data is
reduced considerably, as compared, for example, with the significant changes in the standing
wave if the rocking curve is instead scanned [11].

As a final characterization step after actual spectroscopic measurements, high-resolution
transmission electron microscopy (HRTEM) at a resolution of about 1.6 Å was carried out at
the National Center for Electron Microscopy on sections of multilayer with an Fe/Cr bilayer
grown on top, with this revealing very smooth interfaces having intermixing and/or roughness
over <5–8 Å.

The theoretical calculations used in analysing our photoemission data make use of a
specially written computer program [23] which includes single and multiple x-ray reflections
at the top surface and all buried interfaces, parametrized compositional intermixing at
the interfaces of linear form, several improvements over prior programs for doing such
calculations [24] and all information relevant to quantitatively calculating the depth-dependent
emission of photoelectrons from the structure (e.g. differential photoelectron cross sections [25]
and inelastic electron attenuation lengths [26]) once the depth-dependent exciting electric field
strength squared $(\vec{E}(z)^* \cdot \vec{E}(z) = |\vec{E}(z)|^2)$ is determined via x-ray optics.

As one example of the results obtained, we have analysed the core-level photoemission
intensity ratio I(Cr 3p)/I(Fe 3p) as a function of both x-ray incidence angle $\theta_{h\nu}$ (a rocking curve)

and Cr thickness d_{Cr} so as to derive both the layer thicknesses shown in figure 1(a) and an rms interdiffusion length above the wedge sample of $\sigma^{Fe/Cr} = 3.4$ Å. We have assumed here a linear variation of composition of both species. Measured values for this photoelectron intensity ratio are shown in figure 1(b), and they are in excellent agreement with theory, finally permitting us to determine both the Fe and Cr layer thicknesses (cf figure 1(a)) and the intermixing distances with accuracies of about ± 2.0 Å. Further analysing other core intensities yields a $\sigma^{Cr/C+O+B4C}$ of 3.8 Å between Cr and a surface-reacted C + O + B$_4$C layer of about 10 Å thickness on top of the multilayer, and $\sigma^{C+O+B4C/B4C}$ of 3.1 Å between this reacted layer and the first B$_4$C layer in the multilayer. The first B$_4$C layer thus expands by about 50% on air exposure, a result that we have independently confirmed by STEM images (not shown here) [23]. Very accurate layer thickness and interface mixing measurements are thus possible with the standing-wave photoemission technique, and the thicknesses and degrees of interface mixing are shown in figure 1(c). The final calculated standing-wave strengths $|\vec{E}(z)|^2$ in this particular multilayer + bilayer are also shown in figure 1(c), and they exhibit a very strong modulation from the maximum to only about one-third of this value for our experimental incidence angle, with this modulation decreasing somewhat as the Cr layer becomes thicker, but the standing-wave phase remaining constant. This modulation thus permits selective probing of the interface by scanning the x-ray spot over the wedge-shaped bilayer. As noted above, the standing wave is also primarily a property of the multilayer, as verified by both experiment and calculation, and is negligibly influenced by the growth of the bilayer on top of it, as long as the photon energy is chosen well away from any core-level absorption resonances in the bilayer or multilayer constituents. In figure 1(c), we note that the maximum of the electric field intensity lies at the interface between Fe and Cr for beam position B ($d_{Cr} = 62$ Å) while the minimum of the field lies at the interface for position C ($d_{Cr} = 82$ Å). The 20 Å thickness difference between the two positions represents half of the period of the SWG of 40.5 Å.

We now turn to other spectroscopic measurements via the scanning of the standing wave through the interface, and in figure 2(a), we first show MCD data based on spin–orbit-split Fe 2p$_{1/2,3/2}$ and Cr 2p$_{1/2,3/2}$ photoelectron spectra, with $I_{MCD} = I_{RCP} - I_{LCP}$, and a minimal normalization correction of only a few per cent being needed to bring the left and right background points of I_{RCP} and I_{LCP} to equality. The x positions of the sample were here chosen to have the maximum (position B) and minimum (position C) of the standing wave centred on the interface. Both Fe and Cr show reproducible MCD signals, although that for Fe is much larger, by a factor of about five. The 2p$_{1/2}$ and 2p$_{3/2}$ MCD signals for both elements are also reversed in sign, being roughly mirror images of one another; this is a well known result for such ferromagnetic metals [27] and confirms the accuracy of our measurements. Note also that the signs of the two signals are reversed, with for example the Fe 2p$_{3/2}$MCD going negative, then positive, as binding energy decreases, and the Cr MCD 2p$_{3/2}$ MCD going positive, then negative. Because the MCD measurement has an external spin reference, via the polarization in the incoming x-ray beam, which is very close to parallel (anti-parallel) with the Fe layer magnetization direction for RCP(LCP) radiation, we can thus conclude that Cr shows weak ferromagnetism along the y-direction near the interface, but that the orientation of its magnetization is opposite to that of Fe, a result consistent with prior studies [12, 13]. From these measurements alone, we do not derive any information on other components of the magnetization in the two directions x and z perpendicular to the primary Fe magnetization direction, but with modification of the experimental geometry, scanning in both x and y, and the addition of magnetic linear dichroism (MLD) measurements [23, 28], it should be possible in future experiments to determine the x-, and perhaps also the z-magnetization.

Further confirmation of these MCD results is also found in analogous MCD data for Fe 3p and Cr 3p emission (not shown here) [23]. From both the 2p and 3p MCD data, it can also
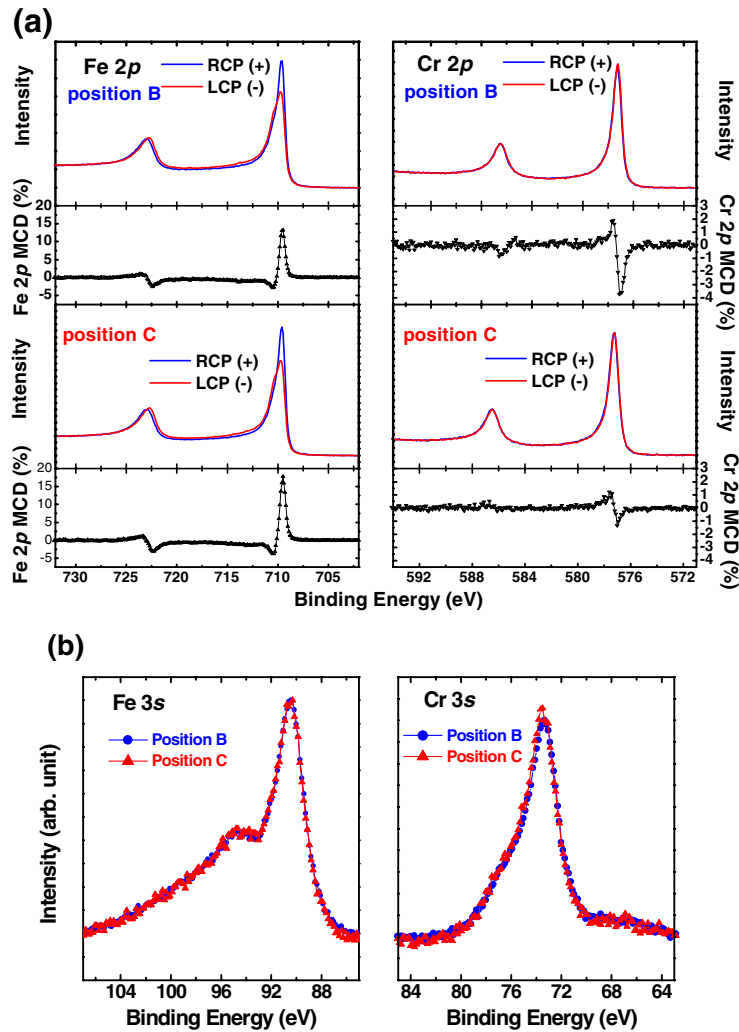
Figure 2. (a) 2p spectra for Fe and Cr for both RCP and LCP excitation, respectively, together with their difference curves (MCD) for the two special x-positions B and C. (b) 3s spectra for Fe and Cr at the same two x-positions. (c) Fe and Cr 2p and 3p MCD results as a function of d_{Cr} (or equivalently of the position of the standing wave with respect to the interface). The experimental data (lines and symbols) are compared with theoretical simulations for the best-fit set of parameters z and σ, as defined in part (d) (solid curves). Vertical black lines represent estimated errors in the MCD measurements. The other curves shown represent some choices at the outside of our estimated error range in determining these parameters. (d) Top panel: model for the variation of composition and y-component of net magnetic moment (magnetization) around the Fe–Cr interface. In the lower panels I and II, the electric field strengths (black solid curve) and distribution of the y-component of ferromagnetic order (blue solid curve: Fe, red solid curve: Cr) are shown as a function of depth from the surface. The single-hatched regions represent Fe (yellow) and Cr (blue) layers while the double-hatched indicate the intermixed region of Fe and Cr. In panels III and IV, the photoelectron intensities from depth z for Fe 2p (blue curves) and Cr 2p (red curves) are shown, and in panels V and VI, the contribution to MCD intensity from depth z due to the ferromagnetic distributions for Fe 2p (blue curves) and Cr 2p (red curves) is plotted. The Cr intensities are amplified for enhanced visibility (compare the left and right ordinates).
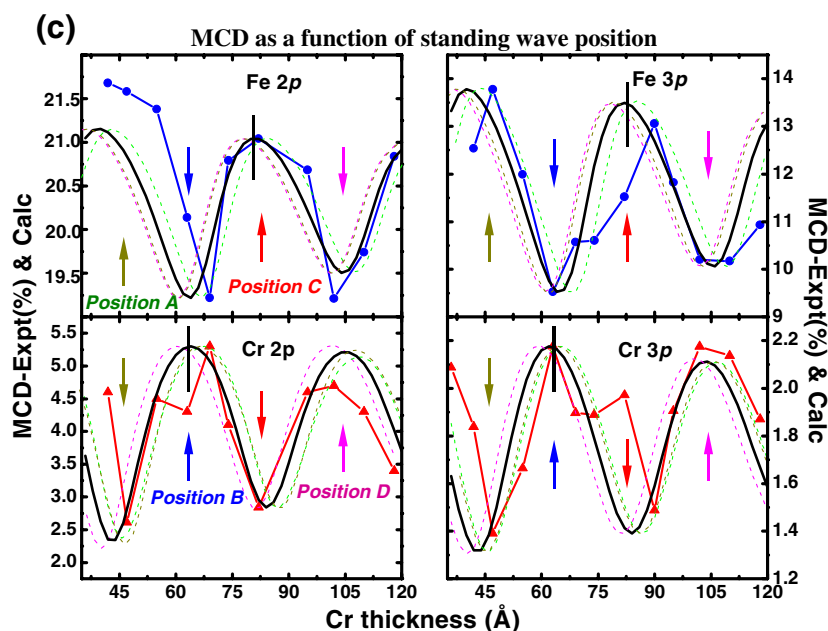
(c)

Figure 2. (Continued.)

be clearly seen that the Fe MCD strength in position B is considerably larger than that in position C, while the Cr MCD shows reverse behaviour. This indicates that any long-range (or even short-range) ferromagnetic order shows a strong dependence on depth near the interface, and that the alterations in the y-component magnetizations of Fe and Cr have very different z-dependence.

We now ask via another spectroscopic fingerprint whether these increases (for Cr) or decreases (for Fe) in the MCD signal in crossing from the Fe to the Cr side of the interface can be associated with a reduction in the local atomic spin moment, which is the dominant contributor to the overall magnetic moment on each atom. In figure 2(b), we show a set of Fe 3s and Cr 3s photoelectron spectra obtained with RCP excitation for the key sample x-positions B and C in figure 1(c). Such 3s spectra should not show MCD, as spin–orbit splitting is not present, but are known to provide a qualitative measure of the local atomic spin moment, with the doublet spacing being proportional to this moment and caused by the 3s core–valence exchange interaction [29]. It can be seen that the splitting (∼4.5 eV for Fe and ∼3.5 eV for Cr) and overall shape of these two spectra are essentially identical, irrespective of position. Other spectra at much finer steps in position confirm this lack of sensitivity to position [23]. The fact that the curves at different positions do not show any systematic differences from one position to another thus immediately indicates that the local spin moments of both Fe and Cr are essentially unchanged on passing into the interface. In particular, the Fe spin moment does not decrease due to its intermixing with Cr, nor does the Cr moment increase due to its proximity to ferromagnetic Fe, although both of these effects have been suggested previously based on thin-film deposition experiments [12, 13, 19]. Finally, we note that this kind of core measurement has an implicit internal spin reference [30], and so provides no information on the exact orientation of these moments in the laboratory reference frame, but simply indicates that the *magnitude* of the spin moment does not change through the interface. Adding an *external* spin detector to the measurement in future studies would yield information on the moment orientation.
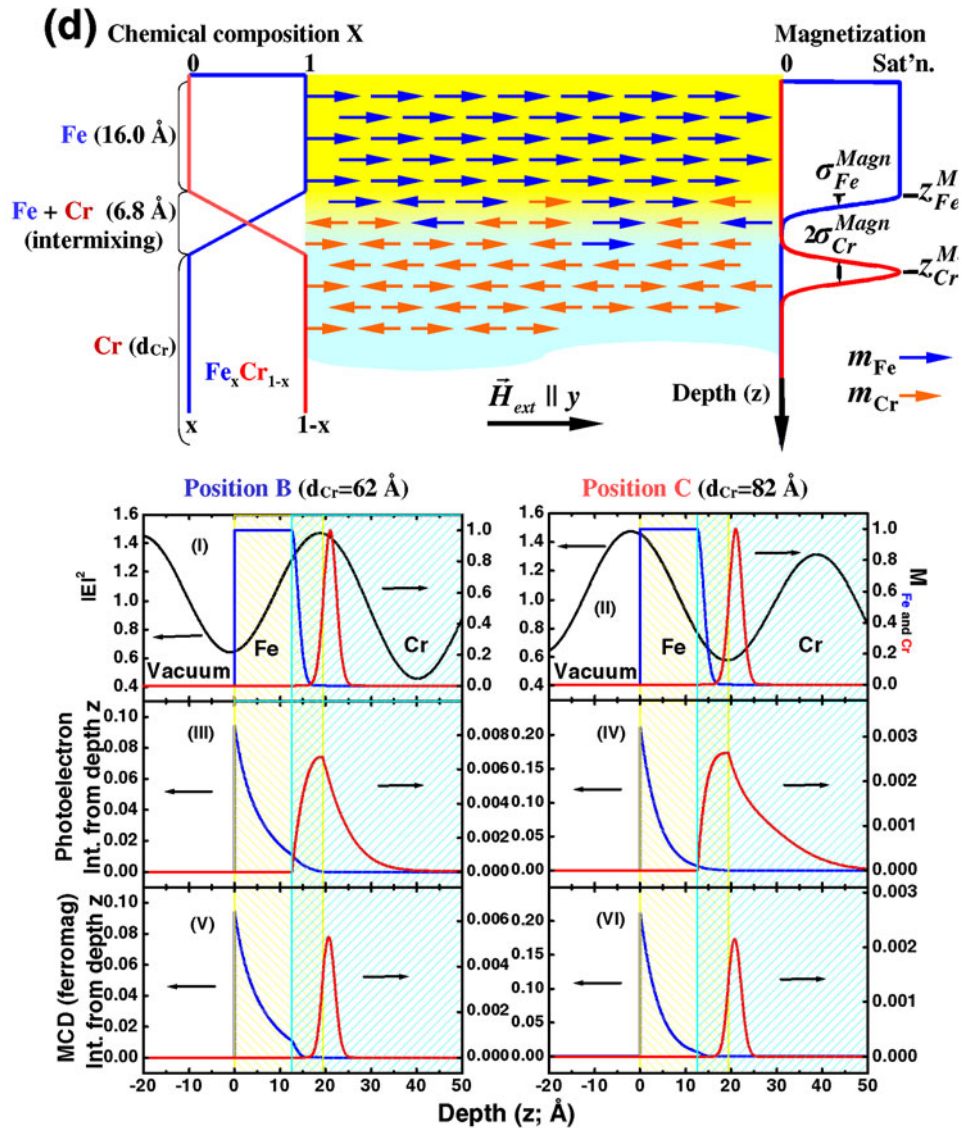
Figure 2. (Continued.)

Turning back to the externally-referenced MCD data, we show in figure 2(c) the experimental variation of the integrated MCD signals for Fe 2p and 3p and Cr 2p and 3p (with a sign change for Cr to permit comparison of relative magnitudes more clearly) as a function of Cr thickness (or equivalently the position of the standing wave relative to the interface). Within estimated experimental errors as shown by the black vertical lines in the figure, there is excellent agreement between the 2p and 3p MCD data for both elements. The positions A, B, C and D of the standing wave (cf figure 1(c)) are also indicated. It is clear from the experimental results that Fe and Cr exhibit very different behaviour across the interface, with Cr showing a maximum in its (negative) dichroism where Fe shows a minimum, and vice versa. Since we know from figure 2(b) that the local atomic spin moments do not change appreciably across

the interface, we can conclude thus far that Cr becomes slightly ferromagnetically ordered on approaching the interface (thus increasing its MCD signal), while the net iron magnetization as seen by MCD is reduced along the reference y direction. This reduction could be due to a random moment alignment, an antiferromagnetic alignment or the existence of a so-called 'spin-flop' transition across the interface in which the Fe moments are aligned along directions to which we are not in this experiment sensitive [31]. Any one of these effects would reduce the present Fe MCD signal.

As a final step in quantifying these results, we now use the measured variation of the Fe and Cr MCD signals with standing-wave position to estimate the positions and thicknesses of the regions over which the Fe shows reduced, and the Cr increased, magnetization. This analysis requires only predicting the *shapes* of the two dichroism curves as a function of depth, rather than their absolute magnitudes. The MCD strengths have been calculated by assuming Gaussian regions of decreased (increased) ferromagnetism for Fe(Cr) near the interface, with the position of the Gaussians (z_{Fe}^{Magn} and z_{Cr}^{Magn}, respectively) and their widths (σ_{Fe}^{Magn} and σ_{Cr}^{Magn}, respectively) being adjustable parameters (cf the top panel of figure 2(d)). Thus, the magnetization of Fe is assumed to have some saturated value well away from the interface and to reduce to zero at least by the point at which its concentration goes to zero, and the Cr is assumed to have zero magnetization except for a Gaussian region somewhere near the interface. The previously measured compositional variation (cf discussion of figure 1(b)) at the interface is thus also included in the calculations. The composition of each constituent and the precise form of the standing wave as calculated via x-ray optics are used as combined weighting factors at each depth for calculating the dichroism signal. We have tried to fit our MCD data with a variety of magnetization configurations for both Fe and Cr, especially around the interface at the middle of which the composition of $Fe_{0.50}Cr_{0.50}$ occurs. The quality of these fits has been assessed both visually and by calculating a reliability factor (R-factor) as $R = \sum_j |I_{expt,j}^{MCD} - I_{calc,j}^{MCD}|^2 / \sum_j [I_{expt,j}^{MCD}]^2$. From this analysis, it is found out that our results cannot be reproduced unless the net y magnetization for both Fe and Cr at the 50:50 intermixing region is essentially zero. This is at least consistent with recent results from element-specific MCD in x-ray absorption for a series of Fe–Cr alloys [32], which indicate that neither Fe nor Cr shows any net magnetization in an $Fe_{0.50}Cr_{0.50}$ alloy. The final most self-consistent and reasonable analysis of both the ratio curves for Fe 3p and Cr 3p (cf figure 1(c)) and the MCD data of figure 2(c) leads to the values of $\sigma_{intermix} = 3.4$ Å, $z_{Fe}^{Magn} = 12.5$ Å, $\sigma_{Fe}^{Magn} = 2.8$ Å and $z_{Cr}^{Magn} = 21.1$, $\sigma_{Cr}^{Magn} = 2.0$ Å and to calculated final forms for the MCD curves as shown by the smooth curves in figure 2(c) (thick black solid curves). There is very good agreement between experiment and theory, if allowance is made for the estimated uncertainty in each MCD value quoted above.

In order to more quantitatively see how sensitive these fits are to these parameters, a few different choices are also illustrated in figure 2(c), in which either the z position or the σ value is changed from the best fit values: $z_{Fe}^{Magn} = 16.5$ Å, $\sigma_{Fe}^{Magn} = 2.8$ Å and $z_{Cr}^{Magn} = 25.1$ Å, $\sigma_{Cr}^{Magn} = 2.0$ Å (green lines); $z_{Fe}^{Magn} = 8.5$ Å, $\sigma_{Fe}^{Magn} = 2.8$ Å and $z_{Cr}^{Magn} = 17.1$ Å, $\sigma_{Cr}^{Magn} = 2.0$ Å (pink lines); and $z_{Fe}^{Magn} = 12.5$ Å, $\sigma_{Fe}^{Magn} = 7.6$ Å and $z_{Cr}^{Magn} = 21.1$ Å, $\sigma_{Cr}^{Magn} = 5.8$ Å (orange lines). These fits show good sensitivity to intermixing width and the forms of the ferromagnetic ordered regions, finally indicating that photoemission spectroscopy via soft x-ray standing-wave excitation can probe buried interfaces with high resolutions in z of the order of $\sim$2–3 Å (about one atomic layer) and in σ of $\sim$4–5 Å (about two atomic layers).

Our final conclusions concerning the variations of both the concentration and magnetization as projected along the x-direction near this Fe–Cr interface are thus as summarized in figure 2(d), where we show not only composition and magnetization, but also

the calculated field strengths and depth-resolved contributions to intensity and MCD for the two key positions B and C. Our results are in agreement with prior work in that MCD effects are reduced in Fe–Cr alloys [32] and that the Cr layers nearest to Fe show some ferromagnetic alignment, but in an antiferromagnetic sense with respect to Fe [12, 13]. However, we can also rule out certain other models and conclusions such as a significant change of the local magnetic moments on either Fe or Cr on passing through the interface. Instead spin-flops or frustrated exchange interactions leading to out-of-plane orientations might explain our results because the MCD measurements pick up the majority of magnetic moments aligned with photon helicity orientation only. It is also remarkable from our analysis that the regions over which Fe or Cr show altered magnetic behaviour along the x-direction are only about two atomic layers in thickness. Although the picture of this interface that emerges is simple in some respects and complex in others, we believe that future modelling of it must take account of these effects. The standing-wave-plus-wedge approach has permitted us to delve into its characteristics in a much more quantitative way.

We have thus demonstrated that the use of synthetic multilayers as generators of strong soft x-ray standing waves and as substrates on which various types of nanostructure can be grown represents a promising method for studying buried interfaces. We have used photoelectrons as the emitted particles, with total intensities, MCD and exchange-split core binding energies providing depth-resolved information with a resolution in the few ångstrom range for composition, net magnetization, and local spin moment at the Fe–Cr interface, respectively. In the future, other experimental geometries, linear dichroism and external spin detection should provide additional dimensions of magnetic sensitivity. Future work could also involve chemical shifts in core binding energies (e.g. in tunnel-junctions [4]), valence-band photoemission spectra (thus probing the bonding electrons and densities of states directly), as well as the emission of soft x-ray photons of greater depth penetration and additional symmetry selectivity via dipole selection rules. Due to the greater penetration depths, looking at soft x-ray emission would have the additonal advantage over photoelectron emission of yielding depth-resolved intensity profiles corresponding to those in panels III and IV of figure 2(d) that would much more closely follow the field strengths shown in black in panels I and II, and thus provide even greater buried interface sensitivity. This technique is particularly simple in interpretation when the nanostructure can be grown in (or on top of) a wedge-shaped geometry, thus permitting a fixed standing wave to be scanned through the interface simply by moving a focused x-ray beam along the wedge. Although the multilayer must have a high x-ray optical contrast to set up a strong standing wave (as e.g. the B_4C/W system studied here), various other combinations of materials should be possible[6]. Growing the multilayer *in situ* under better controlled conditions (rather than *ex situ* with subsequent transfer in air as in our experiments) should also permit achievement of better epitaxy and/or structural control in the final structure to be studied. The structure to be studied also does not have to be layered, but might consist of nanoscale 'wires' or 'dots', in which case the top, side and bottom interfaces of these features could be selectively studied. Combining a multilayer + wedge sample geometry with a spectromicroscope [9] should also lead to enhanced depth resolution with this type of experiment. One limitation of the method is that higher-temperature preparation or annealing of the multilayer plus sample will be limited, as going to a sufficiently high temperature will lead to interdiffusion in the multilayer, with resulting loss of reflection efficiency and standing-wave strength. Nonetheless, various possible future applications of this approach to the study of buried interfaces in nanostructures seem possible.

---

[6] Center for X-Ray Optics, Lawrence Berkeley National Laboratory, summary of multilayer data for various systems at http://www-cxro.lbl.gov/cgi-bin/mldata.pl.

References

[1] Baibich M N, Broto J M, Fert A, Nguyen van Dau F, Petroff F, Etienne P, Creuzet G, Friederich A and Chazelas J 1988 *Phys. Rev. Lett.* **61** 2472
Binasch G, Grünberg P, Saurenbach F and Zinn W 1989 *Phys. Rev.* B **39** 4828
Barthelemy A, Fert A, Baibich M N, Hadjoudj S, Petroff F, Etienne P, Cabanel R, Lwquien S, Nguyen Van Dau F and Creuzet G 1990 *J. Appl. Phys.* **67** 5908
Dieny B, Speriosu V S, Parkin S S P, Gurney B A, Wilhoit D R and Mauri D 1991 *Phys. Rev.* B **43** 1297
Parkin S S P 1993 *Phys. Rev. Lett.* **71** 1641
[2] See overviews in
Parkin S S P 1995 *Annu. Rev. Mater. Sci.* **25** 357
Vouille C, Barthelemy A, Mpondo F E, Fert A, Schroeder P A, Hsu S Y, Reilly A and Loloee R 1999 *Phys. Rev.* B **60** 6710
[3] See overviews in
Nogués J and Schuller I K 1999 *J. Magn. Magn. Mater.* **192** 203
Berkowitz A E and Takano K 1999 *J. Magn. Magn. Mater.* **200** 552
[4] Moodera J S, Kinder L R, Wong T M and Meservey R 1995 *Phys. Rev. Lett.* **74** 3273 and references therein
Prinz G A 1998 *Science* **27** 1660
Parkin *et al* S S P 1999 *J. Appl. Phys.* **85** 5828
[5] Batson P E 1999 *Ultramicroscopy* **78** 33
Muller D A, Sorsch T, Moccio S, Baumann F H, Evans-Lutterodt K and Timp G 1999 *Nature* **399** 758
[6] Sève L, Jaouen N, Tonnerre J M, Raoux D, Bartolomé F, Arend M, Felsch W, Rogalev A, Goulon J and Gautier C 1999 *Phys. Rev.* B **60** 9662
[7] Schad R, Beliën P, Verbanck G, Potter C D, Fischer H, Lefebvre S, Bessiere M, Moshchalkov V V and Bruynseraede Y 1998 *Phys. Rev.* B **57** 13 692
Schmidt C M, Bürgler D E, Schaller D M, Meisinger F, Güntherodt H-J and Temst K 2001 *J. Appl. Phys.* **89** 181
[8] MacKay J F, Teichert C, Savage D E and Lagally M G 1996 *Phys. Rev. Lett.* **77** 3925
Freeland J W, Chakarian V, Bussmann K, Idzerda Y, Wende H and Kao C C 1998 *J. Appl. Phys.* **83** 6290
Freeland J W, Bussmann K, Idzerda Y U and Kao C-C 1999 *Phys. Rev. Lett.* **60** 9923
[9] Ohldag H, Scholl A, Nolting F, Anders S, Hillebrecht F U and Stöhr J 2001 *Phys. Rev. Lett.* **86** 2878
[10] Yang S-H, Mun B S, Kay A W, Kim S-K, Kortright J B, Underwood J H, Hussain Z and Fadley C S 2000 *Surf. Sci. Lett.* **461** L557
[11] Kim S-K and Kortright J B 2001 *Phys. Rev. Lett.* **86** 1347–50
[12] Xu Zhongde, Liu Y, Johnson P D and Itchkawitz B S 1995 *Phys. Rev.* B **52** 15 393
[13] Panaccione G, Sirotti F, Narducci E and Rossi G 1997 *Phys. Rev.* B **55** 389
Rossi G, Panaccione G, Sirotti F, Lizzit S, Baraldi A and Paolucci G 1997 *Phys. Rev.* B **55** 11 488
[14] Davies A, Stroscio J A, Pierce D T and Celotta R J 1996 *Phys. Rev. Lett.* **76** 4175
[15] Schmid C M, Burgler D E, Schaller D M, Meisinger F, Guntherodt H J and Temst K 2001 *J. Appl. Phys.* **89** 181 and references therein
[16] Vega A, Demangeat C, Dreyssé H and Chouairi A 1995 *Phys. Rev.* B **51** 11 546
Freyss M, Stoeffler D and Dreyssé H 1997 *Phys. Rev.* B **56** 6047
[17] Turtur C and Bayreuther G 1994 *Phys. Rev. Lett.* **72** 1557
[18] Polak M, Fadley C S and Rubinovich L *Phys. Rev.* B at press
[19] Hillebrecht F U, Roth Ch, Jungblut R, Kisker E and Bringer A 1992 *Europhys. Lett.* **19** 711
Idzerda Y U, Tjeng L H, Lin H-J, Gutierrez C J, Meigs G and Chen C T 1993 *Phys. Rev.* B **48** 4144
[20] Fadley C S, Van Hove M A, Hussain Z and Kaduwela A P 1995 *J. Electron Spectrosc. Relat. Phenom.* **75** 273
[21] Young A T, Martynov V and Padmore H A 1999 *J. Electron Spectrosc. Relat. Phenom.* **101–103** 885
[22] Henke B L, Gullikson E M and Davis J C 1993 *At. Data Nucl. Data Tables* **55** 34
[23] Mun B S 2001 *PhD Thesis* University of California, Davis
Yang *et al* unpublished results

[24] Windt D L 1998 *Comput. Phys.* **12** 360
[25] Yeh Y Y and Lindau I 1985 *At. Data Nucl. Data Tables* **32** 1
[26] Powell C J, Jablonski A, Tanuma S and Penn D R 1994 *J. Electron Spectrosc. Relat. Phenom.* **68** 605
[27] Baumgarten L, Schneider C M, Petersen H, Schäfers F and Kirschner K 1990 *Phys. Rev. Lett.* **23** 492
      Menchero J G 1997 *Phys. Rev.* B **55** 5505
[28] Menchero J G 1998 *Phys. Rev.* B **57** 993
      Rossi G, Sirotti F, Cherepkov N A, Combet Farnoux F and Panaccione G 1994 *Solid State Commun.* **90** 557
[29] Fadley C S and Shirley D A 1970 *Phys. Rev.* A **2** 1109
      Bagus P S, Freeman A J and Sasaki F 1973 *Phys. Rev. Lett.* **30** 850
      Klebanoff L E and Shirley D A 1986 *Phys. Rev.* B **33** 5301
      Johnson P D 1997 *Rep. Prog. Phys.* **60** 1217
[30] Sinkovic B, Friedman D J and Fadley C S 1991 *J. Magn. Magn. Mater.* **92** 301
[31] Koon N C 1997 *Phys. Rev. Lett.* **78** 4865
[32] Kortright J B, Kim Sang-Kook and Ohldag H 2000 *Phys. Rev.* B **61** 64